

## COVERED IMAGE OF SUPERLENS

Yuan Zhang<sup>1, \*</sup> and Michael A. Fiddy<sup>2</sup>

<sup>1</sup>Centre for Optical and Electromagnetic Research, Zhejiang Provincial Key Laboratory for Sensing Technologies, State Key Laboratory of Modern Optical Instrumentations, Zhejiang University, Hangzhou, China

<sup>2</sup>Center for Optoelectronics and Optical Communications, University of North Carolina at Charlotte, Charlotte, NC, USA

**Abstract**—In this paper, we examine the imaging ability of a planar superlens in both the transverse and vertical dimension. By studying the field patterns of the image from different objects (points and scattering surfaces with subwavelength details) in front of a planar superlens, we show the relation between the transverse and vertical resolutions. We mainly discuss why we cannot get high subwavelength resolution for three dimensions at the same time, and there is a trade-off between the transverse and vertical resolution capabilities which is fundamental in nature for a planar superlens.

### 1. INTRODUCTION

Metamaterials [1–7], whose permittivity and permeability can be designed artificially from negative to positive values, can be engineered to exhibit special electromagnetic responses that do not exist in natural materials. Following the first theoretical work of Veselago [1], Pendry et al. [2, 3] fueled enormous interest in validating a low loss negative index metamaterial. Researchers have made many efforts in trying to fabricate metamaterials in our real world [5] and especially one that would provide these properties at optical frequencies (e.g., [8]). A very interesting and potentially high impact application of artificial metamaterials is their use in the development of an imaging system which could obtain an image resolution of an object beyond the diffraction limit. Super resolved images are important in many areas, but the diffraction limit is a road-block for conventional optical

---

*Received 12 December 2012, Accepted 11 January 2013, Scheduled 18 January 2013*

\* Corresponding author: Yuan Zhang (zhydxx@gmail.com).

instruments. How to get an image with subwavelength details has been the goal for much research over the last 60 years, but appropriately designed negative index materials provide one of the first real opportunities to achieve this physically. Pendry found that if the refractive index of a layer is exactly minus one, it can act as a perfect lens which has the ability to recover, in principle, all the subwavelength information of an object in the image domain [9]. This pioneering work has encouraged immense amounts of research to theoretically design [10–23] or experimentally fabricate [24–30] a super resolution imaging system.

Although many well known experiments have made progress in trying to realize a superlens and some encouraging results have been reported, the main obstacle for the superlens to be applied to real application is that fabrication issues remain a challenge. Further innovations are necessary in order to realize a practically negative index metamaterial with minimal losses [31, 32]. However, when the loss of the metamaterial has been sufficiently diminished (e.g., using gain compensation), do we still need to investigate the performance of a superlens? For most optical imaging systems, research is focused on getting better resolution in all three dimensions, which means that the transverse super resolution is necessary as well as a good depth of focus (i.e., good resolution along the optical axis). Namely, to image an object in three dimensions clearly, we need both good transverse and vertical resolution. Mesa et al. made interesting observations about the viability of getting three dimensional superresolution of a point source using a planar superlens in [33]. In this paper, we will further study the capability of the planar superlens for the purpose of imaging three dimensional object, and investigate the relation between the transverse and vertical resolution capabilities.

## 2. THE DEPTH OF FOCUS OF PLANAR SUPERLENS

The first work on a planar superlens proposed by Pendry [9] has attracted many researchers. We consider the evanescent wave transfer of the EM field scattered by an object containing subwavelength-scale details placed in front of such a planar superlens. For clarity, we begin with point objects located at different positions in front of the superlens (illustrated as points  $A$ ,  $B$  and  $C$  shown in Figure 1). As the properties of the superlens are identical in the plane parallel to the interface of the planar superlens, it is convenient to convert the 3D problem to a 2D one, and we only consider  $s$ -polarized waves since the discussion of the  $p$ -polarization case is similar. We use infinitesimal dipoles to represent these point objects, and Eq. (1) describes its

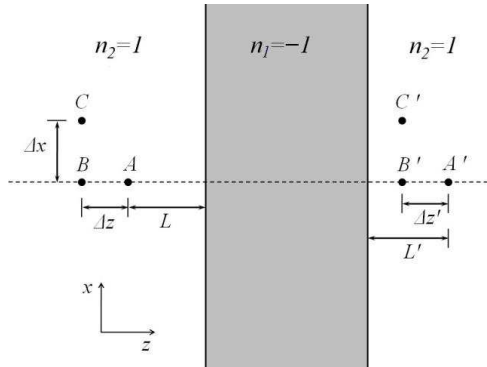


**Figure 1.** Illustration of the planar superlens studied in this paper. The point objects  $A$ ,  $B$  and  $C$  are set at different positions in front of the lens, and the relative distance between them is indicated by  $L$ ,  $L'$ ,  $\Delta x$  and  $\Delta z$ , respectively. The index of the superlens is set to be  $-1$  and the surrounding is air with refractive index  $+1$ .

electric field profile by Fourier expansion. The Fourier components can be divided into propagating waves (with  $|k_x| < k_0$ ) and evanescent waves ( $|k_x| > k_0$ ), where  $k_x$  is the transverse wave vector and  $k_0$  the free space wave vector. To get the super-resolved image, the information carried by the evanescent waves is essential and must be transferred to the image domain in order to replicate the sub-wavelength features of the sources.

$$E = \sum_{k_x} E(k_x) \exp(ik_z z + ik_x x - i\omega t) \tag{1}$$

where  $k_x^2 + k_z^2 = k_0^2$ , with  $-\infty < k_x < +\infty$ .

The superresolution imaging process can be described as follows: at first, the amplitude of each evanescent wave ( $|k_x| > k_0$ ) generated by the point source decreases exponentially when leaving the source position. Once this exponentially decaying evanescent field reaches the left interface of the superlens, its amplitude will increase exponentially when passing through the superlens, and then exponentially decay again when it leaves the lens to the image plane. Consequently, if we need to recover the object perfectly in the image domain, we need the amplitude of each Fourier component of  $k_x$  to equal that at the object plane. This can be fulfilled only when the index of the superlens is impedance matched with the surrounding media (we assume air and  $n_2 = 1$ ), i.e., when  $n_1 = -1$  the lens can form a perfect image of the object [9].

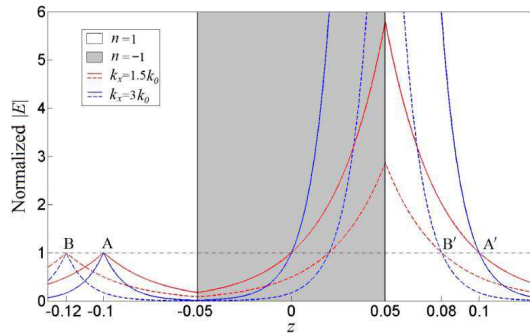


**Figure 2.** The field strength variation of evanescent waves generated by the point objects propagating through the planar superlens to the image position. The evanescent waves generated by point  $A$  are plotted in solid and that of  $B$  in dashed curves. Red and blue colors indicate evanescent waves with transverse wave vectors  $k_x = 1.5k_0$  and  $k_x = 3k_0$ , respectively. We assume that all the evanescent waves have equal normalized field strength at their original position.

We show the evanescent field changing graphically in Figure 2. Suppose that the superlens (with index  $n_1 = -1$ ) is located between  $z = -0.05$  and  $z = 0.05$  (i.e., the thickness of planar lens is 0.1). The operating wavelength is 0.2 in this paper. Here we use unitless parameters for the geometry and wavelength given the scaling law of Maxwell's equations, and the discussion and results are valid for any frequency band. The red and blue solid curves indicate the variation of field strength of the evanescent wave generated by point  $A$  go through the superlens with  $k_x = 1.5k_0$  and  $k_x = 3k_0$ , respectively.

If the index of the superlens is exactly minus one and without any loss, the field strength of every evanescent wave is equal at the position of  $A$  and  $A'$ , and therefore the image at  $A'$  will be perfect. However, this is not the whole story, and we find that the image is somehow not perfect. For a real three dimensional object, we hope to obtain information in all three dimensions, and thus the depth of focus is always an important parameter for an optical instrument. We will mainly examine the depth of focus of the planar superlens using point sources in this part. Suppose that there is another point  $B$  behind point  $A$  (as shown in Figure 1) and that  $\Delta z$  is the distance between  $A$  and  $B$ . According to the imaging principle of the planar negative index lens, we find the image position  $B'$  at  $L_2 = L' - \Delta z$ . We also plot the evanescent field variation generated from point  $B$  in Figure 2 with red and blue dashed curves representing  $k_x = 1.5k_0$  and  $k_x = 3k_0$ ,

respectively. The amplitude of each evanescent wave is assumed to be unity at the original position. We can see that the field strength will decrease exponentially when they leave the point source (decreasing on both sides of  $A$  and  $B$ ), thus indicating there are two peaks at positions  $A$  and  $B$  which ensures the two points can be distinguished clearly. In the image domain, the situation is quite different. For the area before  $A'$  (with positions  $z > 0.1$ ) the field is a perfect copy of that before  $A$  (with position  $-0.05 > z > -0.1$ ), but for the area behind  $A'$  (with positions  $0.1 > z > 0.05$ ) the field distribution is totally different as the field amplitudes are decreasing from a very high level to 1 when they reach  $A'$  from the back interface of the superlens. This evanescent wave behavior results in only the area at  $A'$  being a perfect duplicate of the field at object  $A$ , which is not a real 3D perfect image of the entire object. Another drawback is that all images of the object behind  $A$  will be covered by the “tails” of the field of image  $A'$ . It can be clearly seen from Figure 2 that the front part field of image  $B'$  will be a perfect replica of that of point  $B$  (every evanescent wave will recover to 1 as that of the object), but at the same time the tails of the fields of the evanescent waves from  $A$  going to  $A'$  will be present. For each evanescent wave with  $k_z$ , the field of an evanescent wave of  $A'$  is quite high ( $\exp(k_z \Delta z)$ ), much higher than the recovered field at  $B'$  (as compared to unity). Such a field pattern will make it easy to see that there does not exist two field peaks at  $A'$  and  $B'$  anymore, since the image  $B'$  will be covered by the field of image  $A'$  which makes it hard to distinguish the two points.

With a fixed thickness of the superlens, the “tails” of field of  $A'$  at position  $B'$  are growing exponentially as  $k_z$  increases. This can be seen by comparing the field strength of the red and blue curve in Figure 2 for  $k_x = 1.5k_0$  and  $k_x = 3k_0$ . This indicates that if we want to get a higher transverse (along  $x$  axis) image resolution (i.e., evanescent waves with higher  $k_x$  (and thus higher  $k_z$ ) to be recovered at the image position), the depth of focus of planar superlens will drop more rapidly.

In principle, an infinite number of evanescent waves are generated by a point source (i.e.,  $-\infty < k_x < +\infty$ ), but realistically, the negative index planar superlens has a finite ability to deal with the highest frequency evanescent waves because of the finite size of the unit cell of the metamaterials, or their unavoidable material loss [31, 32]. Such material drawbacks will rapidly diminish the evanescent waves with  $k_x$  larger than a certain threshold  $k_c$ . For clarity we investigated the imaging of points positioned along the  $z$  axis (like  $A$  and  $B$  in Figure 1), here we directly apply a cut-off to the whole range of  $(-\infty < k_x < +\infty)$  to  $(-k_c < k_x < +k_c)$ . This behaves as a special

high transverse wave vector filter which removes all the information carried by evanescent waves with  $|k_x| > k_c$ . In Figures 3(a) and (b), we show the calculated electrical field of different positions along  $z$  axis for  $k_c = 2k_0$  and  $k_c = 5k_0$ , respectively. The red curves in both figures are the field profile at the image plane ( $z = 0.1$ ) of  $A'$ . We can see that the FWHM of the image of  $k_c = 5k_0$  is quite narrow compared with that of  $k_c = 2k_0$ , as more subwavelength information is recovered in Figure 3(b). In Figure 3(a), we also plot the field profile slightly behind  $A'$  at the position  $z = 0.09$  and  $z = 0.075$ , and we can see that the further the position from  $A'$  the higher field strength we get (since it is exponentially growing!). Suppose that the brightness of the two point objects is the same, then any image of  $B$  right behind (no matter how close to)  $A'$  will be covered by the stronger field from  $A'$ , and this is confirmed both in Figures 3(a) and (b). Nevertheless, it is not to say that such a lens will not have any depth of focus at all. For the point-like scatterers having a shift in the lateral direction (e.g., the image of point  $C$  in Figure 1 whose image  $C'$  is not directly behind the

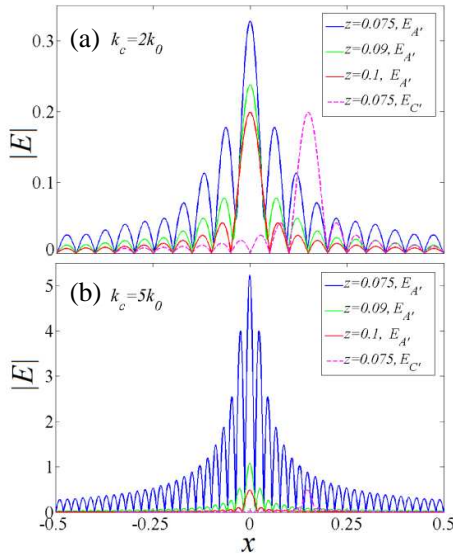


**Figure 3.** Electric field distributions at different position along  $z$  axis for a point object  $A$  located in front of a planar superlens ( $L = 0.1$ ). (a) and (b) are the profiles for  $k_c = 2k_0$ , and for  $k_c = 5k_0$ , respectively. The red curve is the image of point  $A$  under different  $k_c$ , and the dashed pink curve represent the image of point  $C$  in Figure.1 with an  $x$  shift of  $\Delta x = 0.15$ .

image  $A'$ ), there is still a possibility to distinguish them in the image space. When  $k_c$  is small (as in Figure 3(a)), we can see that the field strength of the image  $C'$  is still larger than the tail of  $A'$  at the position of  $z = 0.075$  and  $x = 0.15$ , and therefore it is possible to distinguish the two points having such a position relationship. But this property of depth of focus will become worse very quickly, when  $k_c$  is larger (meaning better transverse subwavelength resolution). This can be confirmed in Figure 3(b), at the position  $z = 0.075$  and  $x = 0.15$ , the image of  $C$  will be buried totally in the overlaid field of  $A'$ . Therefore, if we want to get a higher resolution in the transverse direction (along  $x$  axis), we will necessarily suffer from a worse depth of focus (along  $z$  axis).

The center field strength of the superresolved image  $A'$  can be expressed as:

$$E_{A'} = E_{C'} = \sum_{-k_c < k_x < k_c} E(k_x) \exp(ik_x x_{A'} + ik_z z_{A'} - i\omega t) \quad (2)$$

where,  $(x_{A'}, z_{A'})$  indicates the position of  $A'$ . As point  $C$  has the same brightness as  $A$ , the center field strength of  $C'$  should be equal to that of  $A'$ . Since  $C'$  has a shift of  $\Delta x$ , the field of  $A'$  at the position  $(x_{A'} + \Delta x, z_{A'} - \Delta z)$  is:

$$\begin{aligned} E_p &= \sum_{-k_c < k_x < k_c} E(k_x) \exp(ik_x(x_{A'} + \Delta x) + ik_z(z_{A'} - \Delta z) - i\omega t) \\ &= \sum_{-k_c < k_x < k_c} E(k_x) \exp(ik_x x_{A'} + ik_z z_{A'} - i\omega t) \exp(ik_x \Delta x - ik_z \Delta z) \quad (3) \end{aligned}$$

Therefore, if we want to distinguish  $C'$  from the ‘noise’ of  $A'$ , we need at least:

$$|E_{C'}| > |E_p|$$

From Eq. (3) and Figure 3, we know that the overlapping field  $E_p$  of image  $A'$  decreases as  $\Delta x$  increases, or  $k_c$  decreases, and then larger  $\Delta z$  (i.e., the depth of focus) is allowed, but we know that larger  $\Delta x$  and smaller  $k_c$  mean a reduction of the transverse resolution.

### 3. SUBWAVELENGTH IMAGE OF SCATTERING DIELECTRIC SURFACE

To illustrate more thoroughly the above discussion, next we show some calculations for the image of a scattering surface containing subwavelength details. In Figure 4(a), we put a dielectric bulk object in front of the superlens instead of point sources, and the refractive index of the scattering object is set to 1.5 and the thickness of lens to

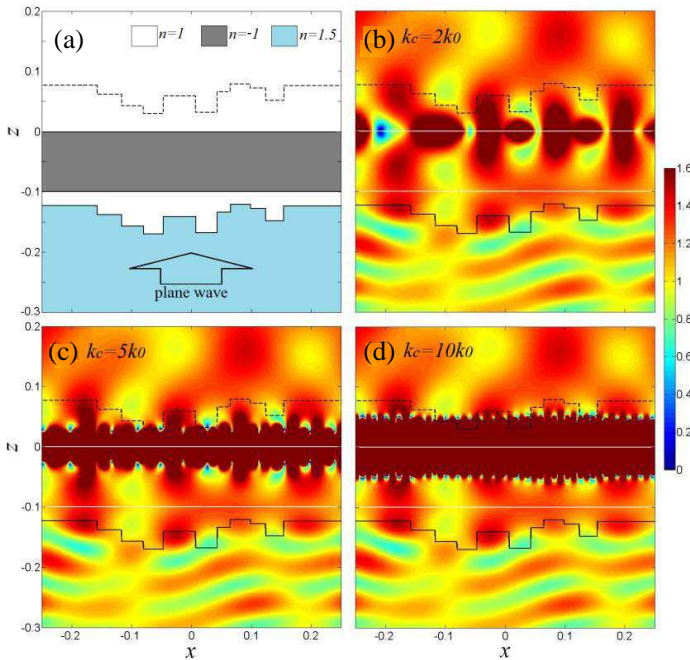


**Figure 4.** (a) Illustrates when a dielectric object (with refractive index 1.5) with stepped surface is located in front of the planar superlens, and illuminated by a plane wave ( $\lambda = 0.2$ ). The dashed curve is the image position of the object surface as determined by the imaging law of planar superlens. (b) to (d) are the  $|E|$  field distributions with different threshold  $k_c$ . As the evanescent wave is growing exponentially when transferring through the superlens, any field strength larger than 1.6 is plotted in dark red to make the distribution easier to see.

0.1. The object has a random stepped surface which has subwavelength details, and is illuminated by a plane wave. Because of the imaging rule for a perfect slab lens, if we take the stepped surface as the object, it should produce an image in the image domain (indicated by the dashed stepped curve in Figure 4(a)). The incident plane wave from bottom of the figure with  $\lambda = 0.2$  is scattered by the rough surface with sub-wavelength features. If a perfect image is formed, the field pattern along the dashed stepped curve should be a copy of that on the object surface. This turns out to be correct, if there is not any disturbance from the imaging of neighboring segments. However, from the discussion in the last section we know this is impossible. In Figures 4(b) to (d) we show the  $|E|$  patterns for  $k_c = 2k_0$ ,  $k_c = 5k_0$

and  $k_c = 10k_0$ , respectively. As the field is growing exponentially on both sides of the upper interface of the planar superlens, the field is plotted in dark red when its strength exceeds 1.6.

From Figure 4, we can see that when  $k_c$  is small, the area of very high field strength (dark red area) does not overlap the image position (dashed curve) that much, and the field pattern close to the dashed curve is still comparable to that of the object surface. When  $k_c$  is growing larger, the dark red area will spread over the dashed curve and swamp the image positions having smaller  $z$  components, and in Figure 4(d) we see that a large part of the image is thus destroyed. But we could also find that the field patterns at the image locations occupying higher (or highest)  $z$  positions and the area beyond them are not affected by the dark red area, which means that the

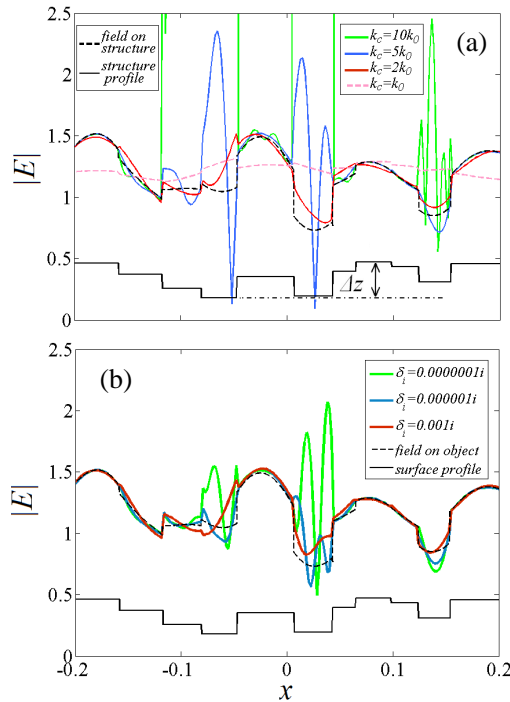


**Figure 5.** (a) Field profile along the image position (dashed curve in Figure 4) for different  $k_c$ , dashed curve is the field distribution on the object surface. (b) Is the case when we use material loss  $\delta$  instead of  $k_c$ . For convenience, the object surface profile is plotted in each figure by the black solid stepped curve.

planar superlens does a perfect job recovering the field patterns of the corresponding object area. In Figure 5(a), we plot the field distribution along the black dashed curve in Figures 3(a)–(b), and for comparison we also plot the field pattern on the object surface in the same picture. The dashed pink curve is the situation  $k_c = k_0$  which means that no subwavelength information is recovered at the image position, thus the image does not show any details of the object. It is clear that when  $k_c$  is larger the image is degraded worse and worse. In Figure 5(b), we also show the calculated results of the field pattern of the image by adding material loss to the negative material instead of using  $k_c$ . The parameter of the negative index material of the superlens is set to  $\varepsilon = -1 + \delta i$  and  $\mu = -1 + \delta i$ . Comparing Figures 5(a) and (b), we can see the same variation of the field pattern at the image position and easily find that a smaller material loss correspond to a larger  $k_c$ . The discussion above means that for a superlens there is an inevitable trade-off between the transverse ( $x$  direction) and vertical ( $z$  direction) resolutions.

In Figure 6, we change the stepped object to a random surface with smooth curvature (the profile of the surface is shown in black solid curves in Figure 6). The drop between the highest peak and deepest valley of the curvature is  $\Delta z = 0.025$  which is half that of the stepped surface in Figure 5 and contains smaller transverse

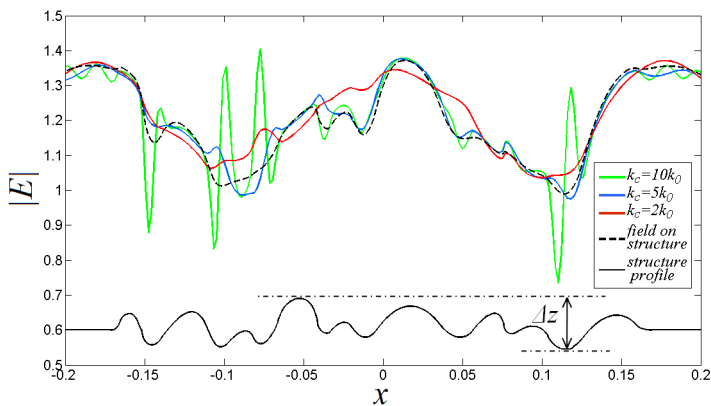


**Figure 6.** Field profile along the image surface for different  $k_c$ , for a dielectric object ( $n = 1.5$ ) with a smooth curvature on its surface (as shown in black solid curve). The imaging system is just the same as in Figure 4(a) except the curved surface replaces the stepped surface. The dashed curve is the field distribution on the object surface. The distance between the highest peak and lowest valley is  $\Delta z = 0.025$ .

subwavelength details. Comparing Figures 5 and 6, we find that with a smaller  $\Delta z$  and lesser high  $k_c$  disturbance, even  $k_c = 10k_0$  does not affect the image that much. In Figure 6, the red curve shows the case of  $k_c = 2k_0$ , and we can see that the image field profile cannot represent the correct object surface because subwavelength information is cut off by the filter  $k_c = 2k_0$ . Similarly for  $k_c = 5k_0$  and  $k_c = 10k_0$ , the subwavelength details can be distinguished at the image position but with a significant disturbance in the image profile corresponding to those lower valleys. This result clearly shows the trade-off between the transverse ( $x$  direction) and vertical ( $z$  direction) resolution.

#### 4. CONCLUSION

To summarize, in this paper we study the depth of focus of a planar superlens to examine its imaging capability when using a three dimensional object. We show that for an object which extends in both the transverse ( $x$ ) and vertical ( $z$ ) dimensions, the object details closest to the front interface of the superlens will destroy the image quality of those object parts behind it. It seems that there is an intrinsic limitation of the planar superlens when imaging an object with a 3D volume perfectly. To image an object with transverse subwavelength details using superlens, we must accept the lower quality of depth of focus. As a result of this trade-off between the transverse ( $x$ ) and vertical ( $z$ ) resolution, one has to make more effort (such as utilizing some computational methods) to assist with improving the superresolution of a three dimensional image when using a planar superlens.

#### ACKNOWLEDGMENT

Yuan Zhang is supported by the National Natural Science Foundation of China (No. 61108022 and No. 61271085), the National High Technology Research and Development Program of China (No. 2012AA030402), and the Program of Zhejiang Leading Team of Science and Technology Innovation. MAF acknowledges support of National Research Foundation of Singapore, grant number NRF-G-CRP 2007-01.

#### REFERENCES

1. Veselago, V. G., "The electrodynamics of substances with simultaneously negative values of permittivity and permeability," *Sov. Phys. Usp.*, Vol. 10, 509–514, 1968.

2. Pendry, J. B., A. J. Holden, W. J. Stewart, and I. Youngs, "Extremely low frequency plasmons in metallic mesostructures," *Phys. Rev. Lett.*, Vol. 76, 4773–4776, 1996.
3. Pendry, J. B., A. J. Holden, D. J. Robbins, and W. J. Stewart, "Magnetism from conductors and enhanced nonlinear phenomena," *IEEE Trans. Microwave Theory Tech.*, Vol. 47, 2075–2084, 1999.
4. Zhang, Y., T. M. Grzegorzczuk, and J. A. Kong, "Propagation of electromagnetic waves in a slab with negative permittivity and negative permeability," *Progress In Electromagnetics Research*, Vol. 35, 271–286, 2002.
5. Shelby, R. A., D. R. Smith, and S. Schultz, "Experimental verification of a negative index of refraction," *Science*, Vol. 292, 77–79, 2001.
6. Kuester, E. F., N. Memic, S. Shen, A. D. Scher, S. Kim, K. Kumley, and H. Loui, "A negative refractive index metamaterial based on a cubic array of layered nonmagnetic spherical particles," *Progress In Electromagnetics Research B*, Vol. 33, 175–202, 2011.
7. Garcia, C. R., J. Correa, D. Espalin, J. H. Barton, R. C. Rumpf, R. Wicker, and V. Gonzalez, "3D printing of anisotropic metamaterials," *Progress In Electromagnetics Research Letters*, Vol. 34, 75–82, 2012.
8. Shalaev, V. M., "Optical negative-index metamaterials," *Nature Photonics*, Vol. 1, 41–48, 2007.
9. Pendry, J. B., "Negative refraction makes a perfect lens," *Phys. Rev. Lett.*, Vol. 85, 3966–3969, 2000.
10. Pendry, J. B. and S. A. Ramakrishna, "Refining the perfect lens," *Physica B: Condensed Matter*, Vol. 338, 329–332, 2003.
11. Ramakrishna, S. A., J. B. Pendry, M. C. K. Wiltshire, and W. J. Stewart, "Imaging the near field," *J. Mod. Optics*, Vol. 50, 1419–1430, 2003.
12. Belov, P. A., Y. Hao, and S. Sudhakaran, "Subwavelength imaging at optical frequencies using a transmission device formed by a periodic layered metal-dielectric structure operating in the canalization regime," *Phys. Rev. B*, Vol. 73, 113110, 2006.
13. Wood, B., J. B. Pendry, and D. P. Tsai, "Directed subwavelength imaging using a layered metal-dielectric system," *Phys. Rev. B*, Vol. 74, 115116, Sep. 2006.
14. Webb, K. J. and M. Yang, "Subwavelength imaging with a multilayer silver film structure," *Opt. Lett.*, Vol. 31, 2130–2132,

- 2006.
15. Feng, S. M. and J. M. Elson, "Diffraction-suppressed high-resolution imaging through metallodielectric nanofilms," *Opt. Express*, Vol. 14, 216–221, 2006.
  16. Shin, H. C. and S. H. Fan, "All-angle negative refraction and evanescent wave amplification using one-dimensional metallodielectric photonic crystals," *Appl. Phys. Lett.*, Vol. 89, 151102, 2006.
  17. Shi, L. H. and L. Gao, "Subwavelength imaging from a multilayered structure containing interleaved nonspherical metallodielectric composites," *Phys. Rev. B*, Vol. 77, 195121, 2008.
  18. Moore, C. P., M. D. Arnold, P. J. Bones, and R. J. Blaikie, "Image fidelity for single-layer and multi-layer silver superlenses," *J. Opt. Soc. Am. A*, Vol. 25, 911–918, 2008.
  19. Cao, P., X. Zhang, L. Cheng, and Q. Meng, "Far field imaging research based on multilayer positive- and negative-refractive-index media under off-axis illumination," *Progress In Electromagnetics Research*, Vol. 98, 283–298, 2009.
  20. Kotyński, R. and T. Stefaniuk, "Multiscale analysis of subwavelength imaging with metal-dielectric multilayers," *Opt. Lett.*, Vol. 35, 1133–1135, 2010.
  21. Jin, Y., "Improving subwavelength resolution of multilayered structures containing negative-permittivity layers by flattening the transmission curves," *Progress In Electromagnetics Research*, Vol. 105, 347–364, 2010.
  22. Yan, C., D. Zhang, Y. Zhang, D. Li, and M. A. Fiddy, "Metal-dielectric composites for beam splitting and far-field deep subwavelength resolution for visible wavelengths," *Opt. Express*, Vol. 18, 14794–14801, 2010.
  23. Cao, P., X. Zhang, W.-J. Kong, L. Cheng, and H. Zhang, "Superresolution enhancement for the superlens with anti-reflection and phase control coatings via surface plasmons modes of asymmetric structure," *Progress In Electromagnetics Research*, Vol. 119, 191–206, 2011.
  24. Fang, N., H. Lee, C. Sun, and X. Zhang, "Sub-diffraction-limited optical imaging with a silver superlens," *Science*, Vol. 308, 534–537, 2005.
  25. Korobkin, D., Y. Urzhumov, and G. Shvets, "Enhanced near-field resolution in midinfrared using metamaterials," *J. Opt. Soc. Am. B*, Vol. 23, 468–478, 2005.
  26. Taubner, T., D. Korobkin, Y. Urzhumov, G. Shvets, and

- R. Hillenbrand, "Near-field microscopy through a SiC superlens," *Science*, Vol. 313, 1595, 2006.
27. Liu, Z., H. Lee, Y. Xiong, C. Sun, and X. Zhang, "Optical hyperlens magnifying sub-diffraction-limited objects," *Science*, Vol. 315, 1686, 2007.
  28. Zhang, X. and Z. Liu, "Superlenses to overcome the diffraction limit," *Nature Materials*, Vol. 7, 435, 2008.
  29. Chaturvedi, P., W. Wu, V. J. Logeswaran, Z. Yu, M. S. Islam, S. Y. Wang, R. S. Williams, and N. X. Fang, "A smooth optical superlens," *Appl. Phys. Lett.*, Vol. 96, 043102, 2010.
  30. Xie, Y., J. Jiang, and S. He, "Proposal of cylindrical rolled-up metamaterial lenses for magnetic resonance imaging application and preliminary experimental demonstration," *Progress In Electromagnetics Research*, Vol. 124, 151–162, 2012.
  31. Smith, D. R., D. Schurig, M. Rosenbluth, S. Schultz, S. A. Ramakrishna, and J. B. Pendry, "Limitations on subdiffraction imaging with a negative refractive index slab," *Appl. Phys. Lett.*, Vol. 82, 1506, 2003.
  32. Stockman, M. I., "Criterion for negative refraction with low optical losses from a fundamental principle of causality," *Phys. Rev. Lett.*, Vol. 98, 177404, 2007.
  33. Mesa, F., M. J. Freire, R. Marqués, and J. D. Baena, "Three-dimensional superresolution in metamaterial slab lenses: Experiment and theory," *Phys. Rev. B*, 72, 235117, 2005.